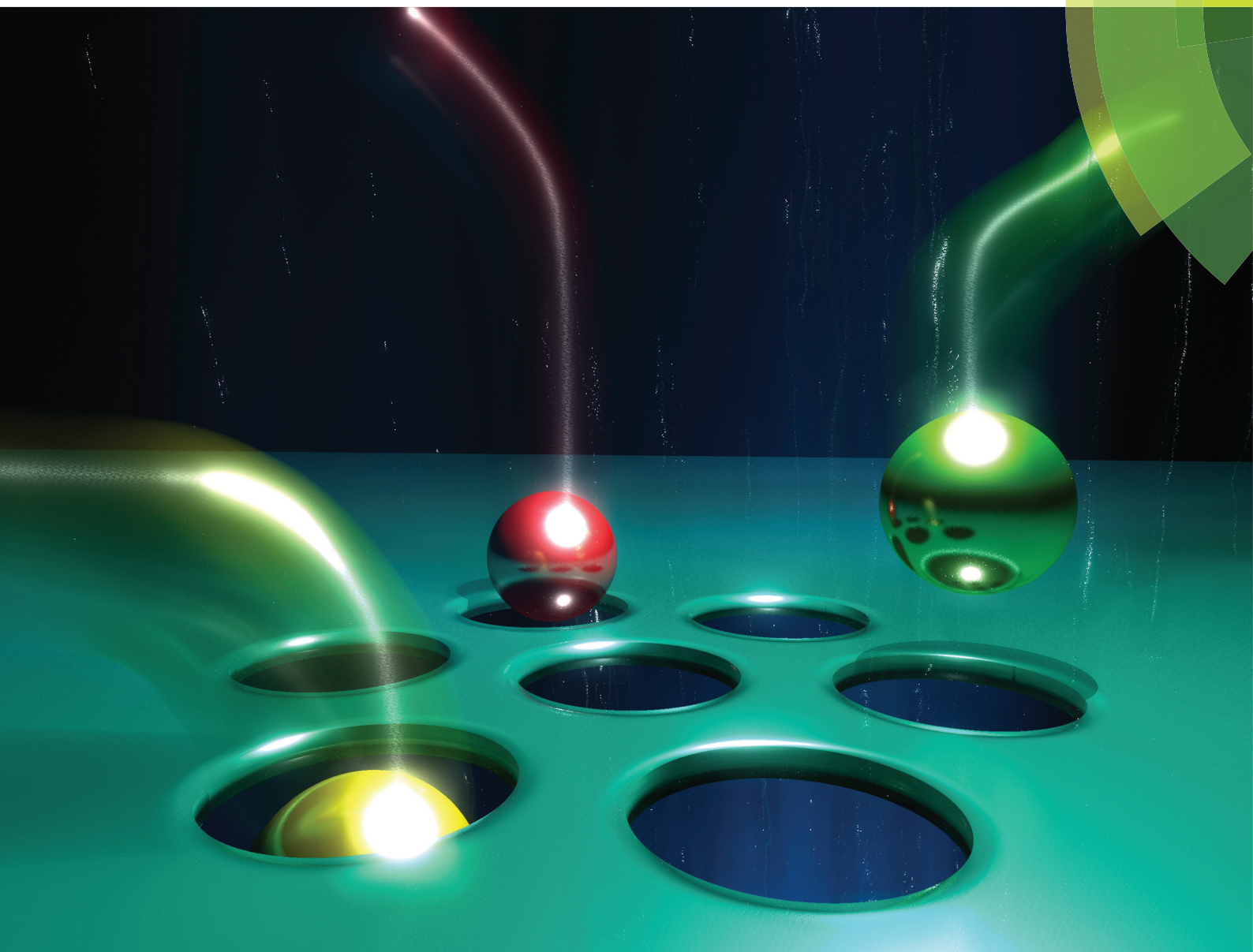# Nanoscale

rsc.li/nanoscale

ROYAL SOCIETY
OF **CHEMISTRY** | Celebrating
IYPT 2019

COMMUNICATION
Makusu Tsutsui, Takashi Washio, Tomoji Kawai *et al.*
Electric field interference and bimodal particle translocation
in nano-integrated multipores

NCNST

Nanoscale

Check for updates

Electric field interference and bimodal particle translocation in nano-integrated multipores†

Makusu Tsutsui, [ID] *[a] Kazumichi Yokota,[a,b] Tomoko Nakada,[a] Akihide Arima, [ID] [a] Wataru Tonomura,[a] Masateru Taniguchi,[a] Takashi Washio*[a] and Tomoji Kawai*[a]

Parallel integration of multiple channels is a fundamental strategy for high-throughput particle detection in solid-state nanopores wherein understanding and control of crosstalk is an important issue for the post resistive pulse analysis. Here we report on a prominent effect of cross-channel electric field interference on the ionic current blockade by nanoparticles in nano-spaced pore arrays in a thin Si_3N_4 membrane. We systematically investigated the variations in resistive pulse profiles in multipore systems of various inter-channel distances. Although each pore acted independently when they were formed at excessively far distances, we observed significant cross-pore electrostatic interactions under close-integration that led the multipores to virtually act as a single-pore of equivalent area. As a result of the interference, the resistive pulse height demonstrated bimodal distributions due to the pronounced particle trajectory-dependence of the ionic blockade effects. Most importantly, the overcrowded multi-channel structure was found to deliver significant crosstalk with serious degradation of the sensor sensitivity to particle sizes. The present results provide a guide to design multipore structures regarding the trade-off between the detection throughput and sensor sensitivity.

Introduction

When an object in electrolyte solution passes through a hole sculpted in a solid membrane, ion transport in the conduit is blocked,[1] which provides a versatile means to count and analyze individual particles and molecules with nanoscale spatial resolution through measuring the associated pulse-like change in the cross-membrane ionic current.[2–7] Yet, the sensor throughput has long been a practical issue since

aThe Institute of Scientific and Industrial Research, Osaka University, Ibaraki, Osaka 567-0047, Japan. E-mail: tsutsui@sanken.osaka-u.ac.jp, washio@ar.sanken.osaka-u.ac.jp, kawai@sanken.osaka-u.ac.jp
bNational Institute of Advanced Industrial Science and Technology, Takamatsu, Kagawa 761-0395, Japan
†Electronic supplementary information (ESI) available: Fig. S1–S9. See DOI: 10.1039/c8nr08632j

the electrical detection can only be implemented by making it possible to draw an analyte into the small channel,[8] wherein a high sample concentration is a prerequisite to have charged objects of concern in the vicinity of the pore for the electrophoretic translocation.[9] In this context, efforts have been devoted to incorporating additional driving forces such as hydrodynamic pressure,[10] salt gradients,[11] electric field gating,[12] and dielectrophoretic mechanisms[13] to control the exterior-channel mass transport for realizing high-throughput detection in a dilute suspension at the expense of complicated electrokinetics involved in the cross-membrane ion transport.[14]

In contrast to these ingenious procedures, drilling and utilizing more than one channels in a membrane is a more straightforward and cost-effective strategy for improving the particle detection efficiency.[15–18] Despite the potential, however, little effort has been devoted to investigating the extent to which the cross-channel interactions affect the ionic blockade characteristics.[19,20] In order to evaluate the potential scalability of this multipore approach, we herein investigated the possible influence of electric field interference among the parallel channels by systematically exploring a change in the resistive pulse profiles by the pore-to-pore distance.

Experimental

Fabrication of multipores

Solid-state multipores were fabricated as follows. First, we partially removed one side of the Si_3N_4 surface of a 25 mm × 25 mm sized piece of a Si_3N_4(50 nm)/Si(500 μm)/Si_3N_4(50 nm) wafer by reactive ion etching (etchant gas: CF_4). The exposed Si layer was then immersed in aq. KOH for deep wet etching. By completely dissolving the Si, we obtained a 50 nm thick Si_3N_4 membrane on the other side. On the membrane, we spin-coated an electron-beam resist (ZEP520A-7). After that, we delineated N circles of diameter 1.2 μm or 300 nm and spacing D_{ch} ranging from 30 nm to 10 μm followed by development.

The residual resist was then used as a mask to sculpt multipores by isotropic CF_4 reactive ion etching. Finally, we removed the residual resist by keeping the substrate in N,N-dimethylformamide overnight and subsequent rinsing in ethanol, isopropanol, and acetone.

Ionic current measurements

The ionic current through multipores was measured as follows. Two blocks of polydimethylsiloxane (PDMS) were adhered on the Si chip containing multiple pores in a Si_3N_4 membrane through activating both the surfaces by an oxygen plasma treatment. On one side of the blocks, we formed a microchannel in advance by imprinting using an SU-8 mold photolithographed on a Si wafer. Also, there were three holes punched in each block. Two of these were used as the inlet and outlet to inject Milli-Q-diluted PBS containing polystyrene nanobeads of diameter d_{PS}. The other one was utilized to place a Ag/AgCl electrode. Using the Ag/AgCl electrodes, we applied a dc voltage of 0.1 V and recorded the cross-membrane current through amplifying the output current with a home-built current preamplifier followed by digitizing at 1 MHz using a fast digitizer (NI-5922).

Data analysis

Resistive pulses were extracted by first offsetting the open pore current in the ionic current traces to zero by subtracting the linearly-fitted component within a time window of 0.5 seconds. We then searched and extracted the pulses having a height larger than 0.2 nA. Finally, we calculated the height I_p and width t_d for further analyses.

Multiphysics simulation

Electric potential distribution, ion transport, and fluid flow in Si_3N_4 multipores were deduced by simultaneously solving Poisson's equation, continuity equation at steady-state current, the Nernst–Planck equation, and the Navier–Stokes equation. The simulations were conducted by a finite element method (FEM) using a software package of COMSOL multiphysics 5.3.[25] The models for single- and double-pores were built on 3-dimensional Cartesian coordinates with a total model size of 30 μm × 30 μm × 30.05 μm. Here, the length 30.05 μm to the membrane normal included the 50 nm thick Si_3N_4 layer.

Results and discussion

Single-nanoparticle detection using Si_3N_4 multipores

Multiple pores of diameter d_{pore} = 1.2 μm were sculpted in a Si_3N_4 membrane of thickness L = 50 nm on a Si wafer by nano-fabrication processes such as electron-beam lithography and reactive ion etching (Fig. 1a).[21] The number of channels N ranged from 1 to 7 with the inter-pore distance D_{ch} varying
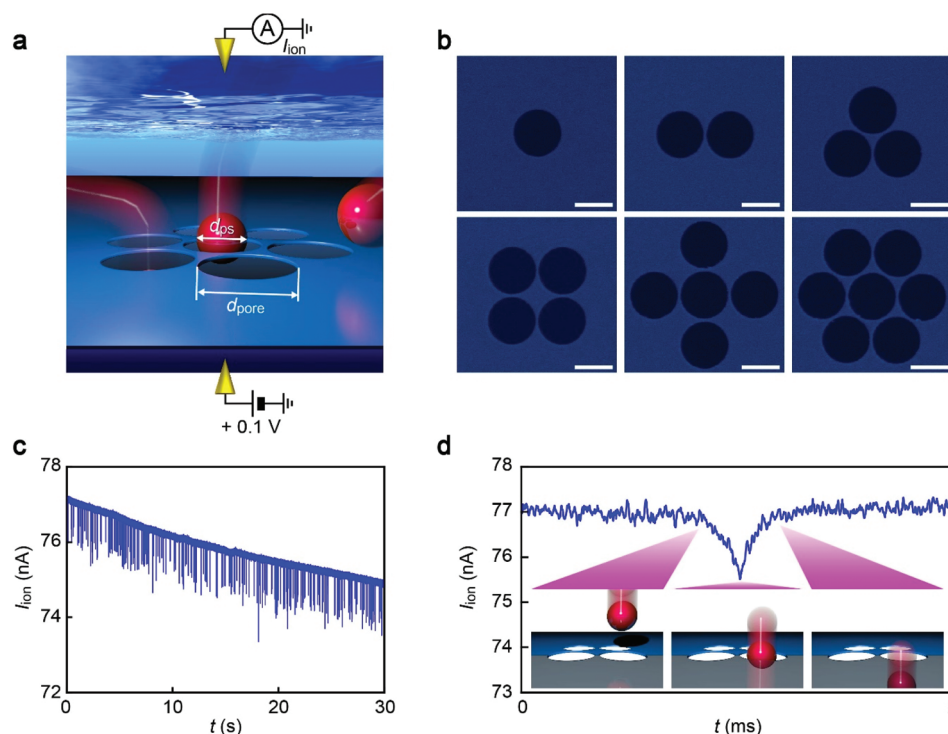
Fig. 1 Single-particle detection using solid-state multipores. (a) Schematic illustration describing a resistive pulse measurement using a Si_3N_4 multi-pore. The cross-pore ionic current I_{ion} was recorded under the applied dc voltage of 0.1 V. (b) False-colored scanning electron micrographs of multi-pores consisting of 1 to 7 pores of diameter 1.2 μm in a 50 nm thick Si_3N_4 membrane. Scale bars denote 1 μm. (c, d) Partial I_{ion} trace obtained with 1.2 μm-sized 4 pores in a dilute dispersion solution of 780 nm-sized carboxylated polystyrene nanoparticles (c). Resistive pulses appeared stochastically representing the translocation of single-particles through one of the four channels (d).

from 100 nm to 10 μm (Fig. 1b; see also Fig. S1†). We measured the ionic current I_{ion} through the micropores under the applied dc voltage of 0.1 V (Fig. S2†) in a suspension of carboxylated polystyrene nanoparticles of diameter d_{PS} in a phosphate-buffered saline (PBS) diluted to 0.2× PBS with ultrapure water (d_{PS} is 780 nm otherwise stated). Irrespective of the multipore arrangements, the ionic current traces showed sporadic emergence of resistive pulses signifying the stochastic nature of single-nanoparticle translocation through one of the N channels (Fig. 1c and d). Interestingly, on the other hand, a conspicuous difference was found in the height I_p of the ionic current signals depending on N and D_{ch} despite the fact that there was no difference in the sizes of the particles nor the pores (Fig. 2a; see also Fig. S3†). In general, I_p reflects the amount of ions excluded by the objects passed through a pore, and hence referred to as a useful index to assess the volume of single particles.[22] Therefore, differing pulse patterns in essentially the same channel geometry for the equi-sized nanobeads manifest an intriguing contribution of crosstalk among the channels on the I_{ion} blockade characteristics.[19,20]

Pore array dependence of resistive pulse heights

The geometrical dependence of the ionic current blockade was further inspected by statistically analyzing I_p distributions (Fig. 2b). As a whole, it was elucidated that whereas I_p approaches the single-pore characteristics under wider separation of the channels, closer positioning of the conduits yields a diminished pulse height down to a level comparable to the equivalent-size single-pore, *i.e.* a 50 nm-long cylindrical channel of diameter $d_{pore} = 1.2N^{0.5}$ μm (Fig. 2c; see also Fig. S4–S5†).

The above results manifest an appreciable influence of electric field interference among the multiple pores.[19] In the low-thickness-to-diameter aspect ratio motif of the channels, the resistance inside the pore $R_{pore} = 4\rho L/\pi d_{pore}^2$ is more than one order of magnitude smaller than that in the exterior regions,[23] which is called access resistance R_{acc} described as $R_{acc} = \rho/d_{pore}$,[24] with the resistivity of the buffer ρ. The applied voltage thus drops largely at the orifices creating a relatively extensive and strong electric field there.[25] More quantitatively, in light of
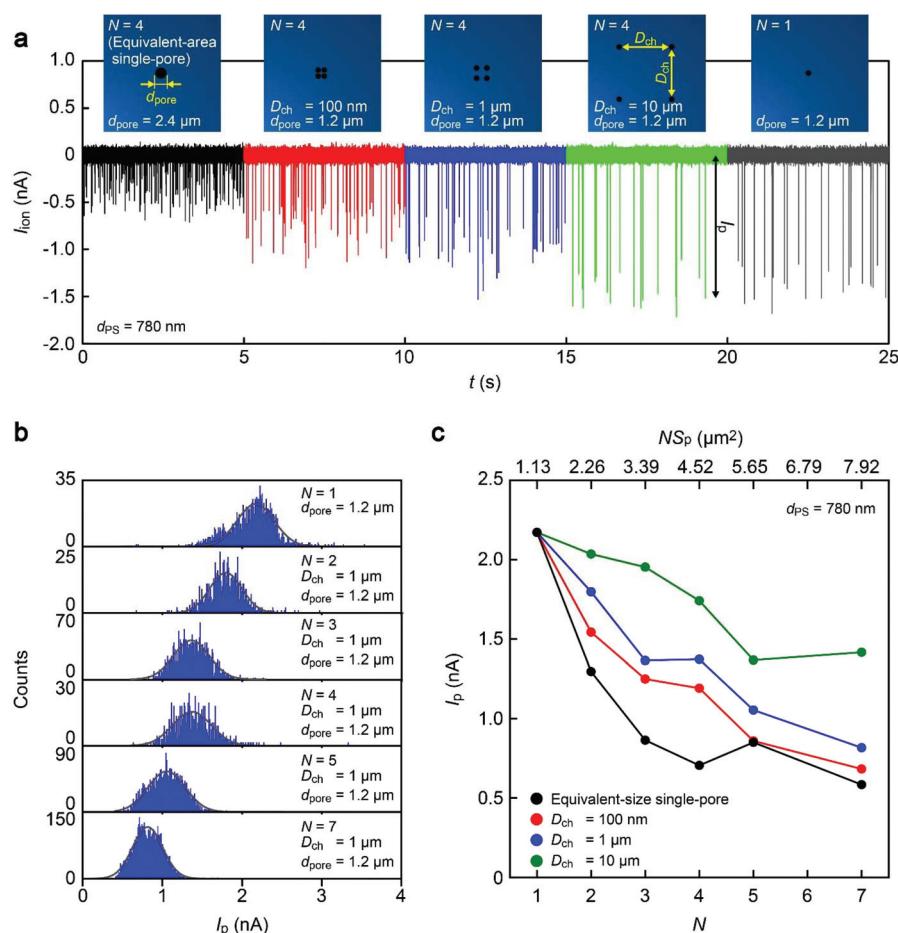
Fig. 2 Ionic current blockade in 1.2 μm-sized multipores. (a) Partial I_{ion} curves in 780 nm-sized particles showing the resistive pulses of varying heights depending on the pore array motifs. (b) Histograms of the pulse height I_p of 1 μm-spaced multipores consisting of 1 to 7 pores. Gray lines are Gaussian fits to the distributions. (c) Dependence of I_p on the number of channels N. Data for the equivalent-area single-pores having an area of NS_p are also shown, where $S_p = 1.13$ μm² is the cross-sectional area of a 1.2 μm-sized micropore (black).

multiphysics simulations, each of the potential profiles at the channels constitute hemispherical distributions equivalent to that in a 1.2 μm-sized pore when disparting the channels enough for electrical isolation of the sensing zone (Fig. S6†).[19] Experimentally, this has been observed as I_p distributions closer to that obtained with the single-micropore at D_{ch} = 10 μm (Fig. 2c) indicating that each conduit worked independently as a single-particle sensor with only marginal effects of the inter-channel interference. In contrast, the fields tend to overlap with each other and converge into one with decreasing pore-to-pore distance thereby affecting the cross-membrane ion transport as well as the single-particle translocation dynamics. Eventually, it infers that the spatially broad fields in low-aspect-ratio multipores would virtually merge them into one of a larger size, as observed in the array-structure dependence of the resistive pulse characteristics in the multiple pore systems (Fig. 2c).

We verified whether the crosstalk persists in multipores of a smaller scale by extending the experiments to 300 nm-sized channels in a 50 nm thick Si_3N_4 membrane. By measuring I_{ion}

in a suspension of carboxylated polystyrene nanoparticles of d_{PS} = 200 nm in 1× PBS, we obtained resistive pulses of diminishing height with the number of channels (Fig. 3a). By examining the statistical distributions of I_p (Fig. 3b), we confirmed a tendency of the pulses to become considerably weaker with increasing N and decreasing D_{ch} (Fig. 3c; see also Fig. S7†), the behavior of which is analogous to that found in the microscale multipores (Fig. 2). This suggests a rather universal feature of the cross-pore interference serving to weaken the ionic blockade effects. It is also worth noting that while the decrease in the pulse height with N becomes quite moderate for D_{ch} = 10 μm, it in turn illustrates the surprisingly expansive nature of the inter-channel interaction that still plays notable roles even when the sensing zones are placed apart by more than a factor of 30 of d_{pore}.

Roles of cross-pore interference on the ionic current blockade

What is distinct between multi- and single-pores from the viewpoints of the ionic current blockade? We addressed this fundamental question by studying the resistive pulse patterns
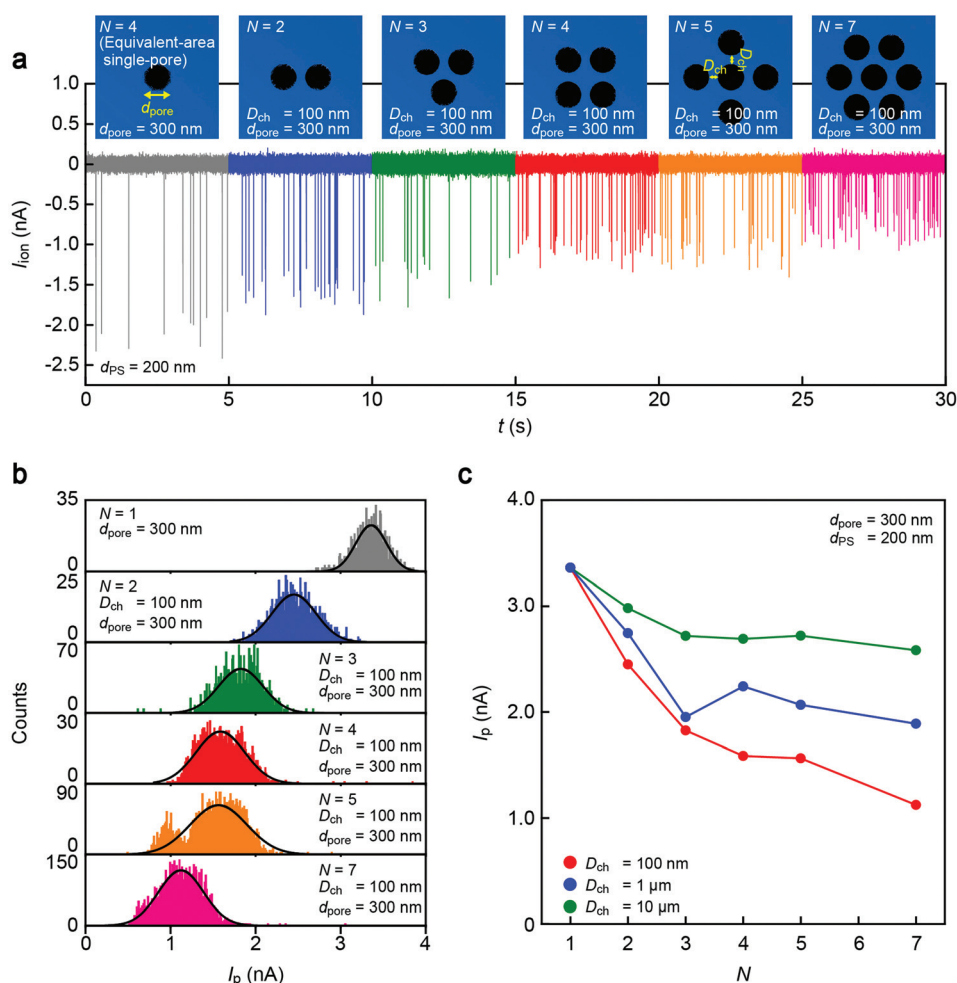
Fig. 3 Array structure-dependent ionic current blockade in multi-nanopores. (a) Partial ionic current traces obtained in a suspension of 200 nm diameter polystyrene nanoparticles using 300 nm-sized multipores with the inter-channel spacing D_{ch} of 100 nm. (b) I_p histograms of the 100 nm-spaced multi-nanopores. Solid curves are Gaussian fitting to the distributions. (c) I_p dependence on N for the multi-nanopores.
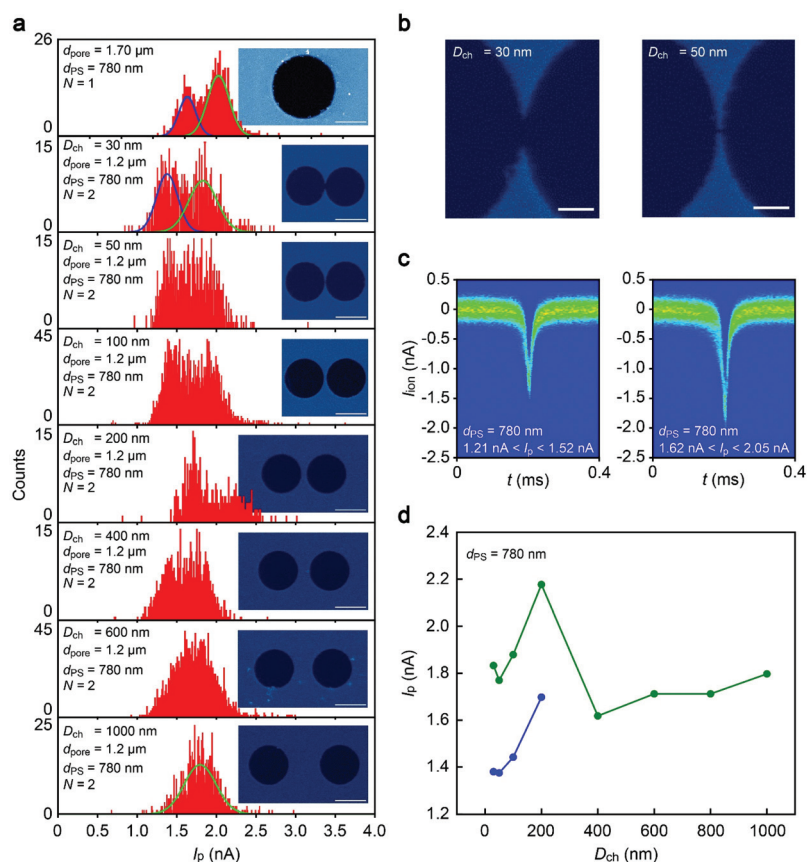
Fig. 4 Bimodal resistive pulse height distributions in nano-spaced double-pores. (a) I_p histograms of double-pores having varying inter-channel spacing D_{ch}. Solid curves are Gaussian fitting to the distributions: green = single-peak; blue = additional peak. The insets are the electron microscopy images of multipores used (white bars denote 1 μm). (b) Scanning electron micrographs showing the ultra-narrow separation wall between the two pores in the case of D_{ch} = 30 nm (left) and 50 nm (right). White bars scale 200 nm. (c) Two-dimensional histograms of the resistive pulses corresponding to the lower (left) and higher (right) I_p states observed in the 30 nm-spaced double pore. (d) Plots of the dual I_p-states in the double pores of various D_{ch}. Green and blue circles denote the higher and lower I_p in the bimodal histograms in (a). Only one peak was observed in the case when the channels were separated by more than 400 nm.

in double-pores of various inter-pore distances from 1 μm to 30 nm (Fig. 4a). Note that the ultra-narrow Si_3N_4 beam between the two channels at D_{ch} = 30 nm was non-suspendable so that the actual structure comprises a single-pore of a non-circular shape, while the separation wall existed in the double-pores of $D_{ch} \geq$ 50 nm (Fig. 4b). Surprisingly, the I_{ion} signal heights demonstrated marked dependence on the inter-channel distance conditions: although the I_p histograms present single-peak structures at large D_{ch}, they start to exhibit bimodal distributions as the spacing was made smaller (Fig. 4a–d; see also Fig. S8–S9†). This finding illustrates detrimental yet unique characteristics of an ionic blockade in multipore systems.

Bimodal distributions of the resistive pulse height

It is of interest to unveil the physics underlying the anomalous distributions of the resistive pulse height in the close-proximity double-pores. As only one kind of polymeric nanobead was dispersed in the buffer, the distinct I_p states cannot be attributed to any variations in d_{PS}. Moreover, there was only

negligible difference in the size of the lithographically-defined two closely-separated channels, less than 1% in d_{pore}, and thus unrealistic to consider any noticeable contribution of the non-uniformity of the pore geometries on the I_{ion} signal height variations (Fig. 1b and S1†). In a similar sense, on the other hand, it would happen that one of the micropores was inadvertently clogged by a nanoparticle during the measurements, whereby it acted as a single-pore thereafter to provide resistive pulses of higher I_p than those in the double-channels. Nonetheless, this was also found not the case by confirming no change in the open pore current I_{open} nor notable dependence of I_p on I_{open} that are suggestive of the channel clogging (Fig. S10†). Therefore, the bimodal I_p is an intrinsic feature stemming from the ionic current blockage by single-particles in the field-interfering multipores.

Being an electrokinetic phenomenon unique in the multi-channel structure, it is worth noting that the dual-state characteristics became even more pronounced when D_{ch} was diminished down to 30 nm whereat the sensor motif was no longer double-pores but a dumbbell-like single-channel (Fig. 4b).

This suggests minor importance of the separation wall between the channels on the ionic blockade characteristics in nano-integrated multipores.

Interference-derived "merging" of dense-integrated multipores

Particle-trajectory-dependence of the ionic current blockade can be a possible explanation for the bimodal I_p distributions.[26] When an object passes through off-center positions, the induced inhomogeneity in the electric field distributions compared to that in the axial translocation leads to more efficient blockage of the ion transport, or equivalently resistive pulses of larger height.[26–29] Multiphysics simulations indeed elucidated higher I_p with a spherical nanoparticle residing at a vicinity of (10 nm from) the side wall of one of the double-pores separated by 100 nm compared to the center-position counterpart (Fig. 5a). Intriguingly, the off-axis contribution was asymmetric in nature, which is significant only when the bead is at the outer side of the double-pore wherein the blockage current is larger by 27% compared to the case for the axial translocation. With the particle at the inner side of the double pore edge, on the other hand, I_p turns to be lower by 5%. The

overall off-axis-effect-derived 32% variation in the blockade current is in quantitative agreement with the bimodal I_p distributions showing peaks at current levels varying by around 25% (the overestimation can be attributed to the actual off-axis paths of the particles taken in the experiments that are seemingly not so close as 30 nm from the wall surface).

The radial-position-dependent ionic current blockade in the double-pore strongly suggests that the closely-spaced pores can be considered as a single-pore of the corresponding cross-sectional area: the inner (outer) side of the multipores corresponds to the center (edge) of the equivalent-area single pore giving smaller (larger) current blockage due to the off-axis effect (Fig. 5b). More directly, the bimodal I_p distributions observed in the close-spaced multipores were also present in the equivalent-area single-pores (Fig. 4a, see also Fig. S11–S12†). The results indicated that the particles tend to pass through the axial positions more frequently as the relative size of the channels becomes larger. Hence, due to the off-axis contributions, the resulting I_p variations demonstrate a double-peak profile. These theoretical results serve to corroborate the role of the electric interference to combine the multiple
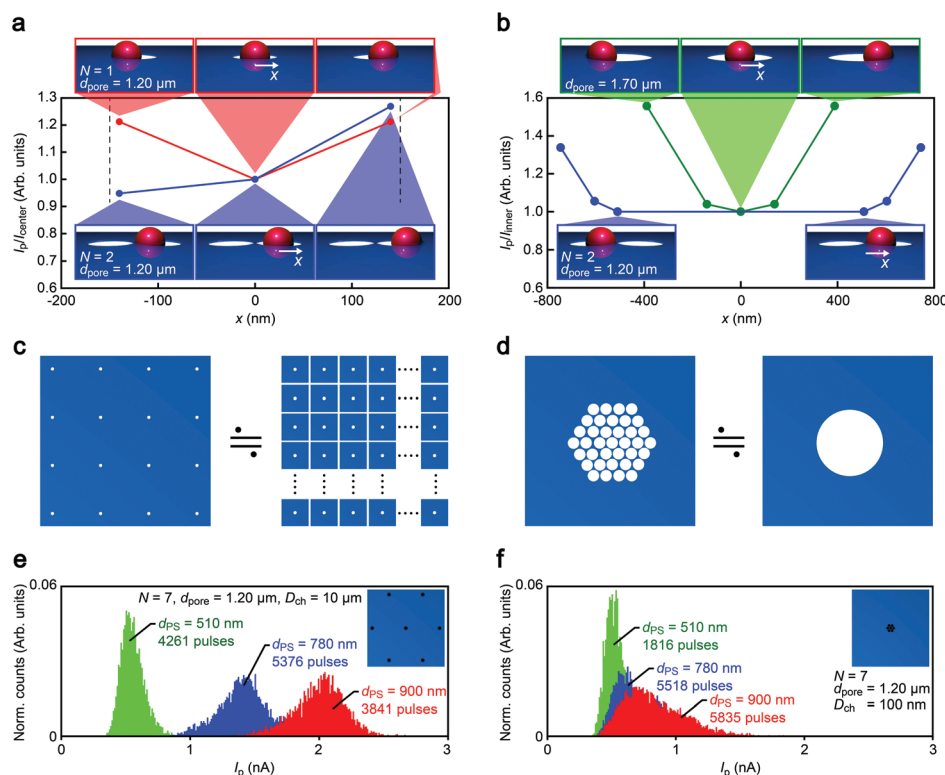
Fig. 5 Particle-trajectory-dependent ionic current blockade in multipores. (a) Multiphysics simulations of the radial position-dependent ionic current blockade by a 900 nm-sized sphere residing in 1.2 μm-sized single (red) and double (blue) pores in a 50 nm-thick Si_3N_4 membrane. x scales the distance from the center of one of the pores along a radial direction. (b) Comparison of the off-axis effects in a double-pore (blue) and the equivalent area single-pore (green). I_p is normalized by I_{inner} defined as the blockade current by the particle occluding 10 nm from the inner-side wall and the center position for the double-pore and the equivalent-area single-pore, respectively. x denotes the distance from the middle of the double-pore corresponding to the center position of the equivalent-area single-pore. (c, d) Schematic illustrations explaining that whereas the N-multipores of diameter d_{pore} with large separation can be regarded as N independent d_{pore}-sized pores (c), close integration entails significant crosstalk that virtually merges the channels into a single-pore of diameter $N^{0.5}d_{pore}$ (d). (e, f) I_p distributions of 510 nm, 780 nm, and 900 nm-sized polystyrenes in 1.2 μm-sized multipores of N = 7 with D_{ch} = 10 μm (e) and 100 nm (f).

sensing zones of multipores into a large single-channel (Fig. 5c and d). In fact, this physical picture is consistent with Fig. 2c displaying similar decay in I_p with N for the short-D_{ch} multipores to that in the equivalent single-pore.

In terms of the sensor capability, the above finding cautions not to make the inter-channel spacing too short so that the resulting interference would not entail severe deterioration of the signal-to-noise ratio to pose critical difficulty for discriminating target analytes. This can be clearly seen in the I_p histograms of three nanoparticles of different sizes, d_{PS} = 900 nm, 780 nm, and 510 nm, demonstrating larger overlaps among the monomodal distributions for 1.2 μm-sized multipores of shorter D_{ch} (Fig. 5e and f). The pore array structure should therefore be designed appropriately to cope with the trade-off in the particle discriminability and the detection throughput.

Conflicts of interest

There are no conflicts to declare.

Acknowledgements

Notes and references

1 W. H. Coulter, *US patent*, 2656508, 1953.
2 S. Iqbal and R. Bashir, *Nanopores: Sensing and Fundamental Biological Interactions*, Springer, 2011.
3 W. Shi, A. K. Friedman and L. A. Baker, *Anal. Chem.*, 2016, **89**, 157–188.
4 L. Luo, S. R. German, W.-J. Lan, D. A. Holden, T. L. Mega and H. S. White, *Annu. Rev. Anal. Chem.*, 2014, **7**, 513–535.
5 D. Branton, D. W. Deamer, A. Marziali, H. Bayley, S. A. Benner, T. Butler, M. Di Ventra, S. Garaj, A. Hibbs, X. Huang, S. B. Jovanovich, P. S. Krstic, S. Lindsay, X. S. Ling, C. H. Mastrangelo, A. Meller, J. S. Oliver, Y. V. Pershin, J. M. Ramsey, R. Riehn, G. V. Soni, V. Tobard-Cossa, M. Wanunu, M. Wiggin and J. A. Schloss, *Nat. Biotechnol.*, 2008, **26**, 1146–1153.
6 S. Howorka and Z. Siwy, *Chem. Soc. Rev.*, 2009, **38**, 2360–2384.
7 D. G. Haywood, A. Saha-Shah, L. A. Baker and S. C. Jacobson, *Anal. Chem.*, 2011, **6**, 615–624.
8 Y. He, M. Tsutsui, M. Taniguchi and T. Kawai, *J. Mater. Chem.*, 2012, **22**, 13423.
9 E. H. Trepagnier, A. Radenovic, D. Sivak, P. Geissler and J. Liphardt, *Nano Lett.*, 2007, **7**, 2824–2830.
10 J.-L. Fraikin, T. Teesalu, C. M. McKenney, E. Ruoslahti and A. N. Cleland, *Nat. Nanotechnol.*, 2011, **6**, 308–313.
11 M. Wanunu, W. Morrison, Y. Rabin, A. Y. Grosberg and A. Meller, *Nat. Nanotechnol.*, 2010, **5**, 160–165.
12 Y. He, M. Tsutsui, C. Fan, M. Taniguchi and T. Kawai, *ACS Nano*, 2011, **5**, 8391–8397.
13 K. J. Freedman, L. M. Otto, A. P. Ivanov, A. Barik, S.-H. Oh and J. B. Edel, *Nat. Commun.*, 2016, **7**, 10217.
14 M. Puster, A. Balan, J. A. Rodriguez-Manzo, G. Danda, J.-H. Ahn, W. Parkin and M. Drndic, *Small*, 2015, **11**, 6309–6316.
15 J. Zhe, A. Jagtiani, P. Dutta, J. Hu and J. Carletta, *J. Micromech. Microeng.*, 2007, **17**, 304–313.
16 S. Huang, M. Romero-Ruiz, O. K. Castell, H. Bayley and M. I. Wallace, *Nat. Nanotechnol.*, 2015, **10**, 986–992.
17 Y. Green, S. Park and G. Yossifon, *Phys. Rev. E: Stat., Nonlinear, Soft Matter Phys.*, 2015, **91**, 011002.
18 M. J. Kim, M. Wanunu, D. C. Bell and A. Meller, *Adv. Mater.*, 2006, **18**, 3149–3153.
19 M. U. Raza, S. Saleem, W. Ali and S. M. Iqbal, *J. Appl. Phys.*, 2016, **120**, 064701.
20 A. Gadaleta, C. Sempere, S. Gravelle, A. Siria, R. Fulcrand, C. Ybert and L. Bocquet, *Phys. Fluids*, 2014, **26**, 012005.
21 M. Tsutsui, S. Hongo, Y. He, M. Taniguchi, N. Gemma and T. Kawai, *ACS Nano*, 2017, **6**, 3499–3505.
22 D. Kozak, W. Anderson, R. Vogel, S. Chen, F. Antaw and M. Trau, *ACS Nano*, 2012, **6**, 6990–6997.
23 S. Garaj, W. Hubbard, A. Reina, J. Kong, D. Branton and J. A. Golovchenko, *Nature*, 2010, **467**, 190–193.
24 J. E. Hall, *J. Gen. Physiol.*, 1975, **66**, 531–532.
25 M. Tsutsui, T. Yoshida, K. Yokota, H. Yasaki, T. Yasui, A. Arima, W. Tonomura, K. Nagashima, T. Yanagida, N. Kaji, M. Taniguchi, T. Washio, Y. Baba and T. Kawai, *Sci. Rep.*, 2017, **7**, 17371.
26 M. Tsutsui, Y. He, K. Yokota, A. Arima, S. Hongo, M. Taniguchi, T. Washio and T. Kawai, *ACS Nano*, 2016, **10**, 803–809.
27 W. R. Smythe, *Rev. Sci. Instrum.*, 1972, **43**, 817.
28 Z. Qin, J. Zhe and G.-W. Wang, *Meas. Sci. Technol.*, 2011, **22**, 045804.
29 E. Weatherall, P. Hauer, R. Vogel and G. R. Willmott, *Anal. Chem.*, 2016, **88**, 8648–8656.